HHS Public Access

Author manuscript

Nat Chem Biol. Author manuscript; available in PMC 2015 August 17.

Published in final edited form as:

Nat Chem Biol. 2013 August ; 9(8): 507–513. doi:10.1038/nchembio.1271.

Side pockets provide the basis for a new mechanism of Kv channel–specific inhibition

Stefanie Marzian[1], **Phillip J Stansfeld**[2], **Markus Rapedius**[3], **Susanne Rinné**[1], **Ehsan Nematian-Ardestani**[3], **Jennifer L Abbruzzese**[4], **Klaus Steinmeyer**[5], **Mark S P Sansom**[2], **Michael C Sanguinetti**[4], **Thomas Baukrowitz**[3], and **Niels Decher**[1,*]

[1]Institute for Physiology and Pathophysiology, University of Marburg, Marburg, Germany

[2]Structural Bioinformatics and Computational Biochemistry Unit, University of Oxford, Oxford, UK

[3]Physiological Institute, University of Kiel, Kiel, Germany

[4]Nora Eccles Harrison Cardiovascular Research and Training Institute, University of Utah, Salt Lake City, Utah, USA

[5]Sanofi-Aventis, Therapeutic Strategic Unit–Aging, Frankfurt, Germany

Abstract

Most known small-molecule inhibitors of voltage-gated ion channels have poor subtype specificity because they interact with a highly conserved binding site in the central cavity. Using alanine-scanning mutagenesis, electrophysiological recordings and molecular modeling, we have identified a new drug-binding site in Kv1.x channels. We report that Psora-4 can discriminate between related Kv channel subtypes because, in addition to binding the central pore cavity, it binds a second, less conserved site located in side pockets formed by the backsides of S5 and S6, the S4–S5 linker, part of the voltage sensor and the pore helix. Simultaneous drug occupation of both binding sites results in an extremely stable nonconducting state that confers high affinity, cooperativity, use-dependence and selectivity to Psora-4 inhibition of Kv1.x channels. This new mechanism of inhibition represents a molecular basis for the development of a new class of allosteric and selective voltage-gated channel inhibitors.

Ion channels are major drug targets for human diseases, in recent years validated by description of numerous human monogenetic ion channelopathies. Voltage-gated potassium (Kv) channels are under investigation as therapeutic targets for cardiac arrhythmias and a variety of neurodegenerative and neuroinflammatory diseases[1]. However, a major limitation

*decher@staff.uni-marburg.de.

Author contributions

N.D. conceived the study. S.M. performed the majority of the experiments. P.J.S. and M.S.P.S. performed the ligand dockings and MDSs. M.R., E.N.-A. and T.B. performed the inside-out macropatch clamp experiments. J.L.A. and M.C.S. performed the cut-open oocyte Vaseline gap measurements. S.R. and S.M. acquired funding. N.D., M.C.S., T.B., S.R., K.S. and S.M. wrote the manuscript.

Competing financial interests

The authors declare no competing financial interests.

Additional information

Supplementary information is available in the online version of the paper. Reprints and permissions information is available online at http://www.nature.com/reprints/index.html. Correspondence and requests for materials should be addressed to N.D.

in drug development is the design of small compound inhibitors of voltage-gated channels that have high subtype specificity.

Most known small-molecule inhibitors of Kv channels bind a cavity below the selectivity filter that is formed by residues located at the base of the selectivity filter and by pore-lining amino acids of the inner (S6) helices. The critical residues are highly conserved in Na^+ and Ca^{2+} channels[2–5] and in Kv channels[6–9], greatly challenging the discovery and development of subtype-specific channel inhibitors. In contrast, peptide toxin inhibitors that either modify gating or occlude the channel pore by binding the outer vestibule often have high subtype specificity because they have a rather large contact interface with extracellular regions of the channels that are not highly conserved[10,11]. However, peptide toxins are of limited practical value for chronic treatment as they require parenteral administration.

By combining comprehensive alanine-scanning mutagenesis, *in silico* drug docking, molecular dynamic simulation (MDS) and patch clamp electrophysiology, we identified a new and nonconserved drug-binding site in the 'side pockets' of Kv channels. We found that drug binding to these side pockets and simultaneous drug binding to the central pore cavity induces an extremely stable nonconducting state in Kv1 channels. This new inhibitory mechanism provides a new approach to develop small-molecule inhibitors with the desired properties of strong use-dependence and channel specificity.

RESULTS

Characterization of Psora-4 affinity and Kv1 specificity

The typical central cavity drug-binding site in Kv1–4 channels is highly conserved (Fig. 1a)[6]. Unexpectedly, Psora-4 selectively blocks Kv1.3 and Kv1.5 with a half-maximum inhibitory concentration (IC_{50}) of 3 nM and 7 nM, respectively, whereas other K^+ channels, including the related Kv3.1, are only blocked in the micromolar range[12]. Although the binding site of PAP-1, an analog of Psora-4, has been described for the Kv1.3 channel[13], the molecular basis of the Kv1.x channel specificity of Psora-4 was unknown. Using *Xenopus* oocytes as an expression system, we confirmed that several Kv1 subfamily members (Kv1.1, Kv1.2, Kv1.5 and Kv1.6) were much more sensitive to inhibition by Psora-4 than Kv2.1, Kv3.1 and Kv4.3 (Fig. 1b and Supplementary Results, Supplementary Table 1). The Hill coefficient of 2.81 ± 0.61 for the concentration-response relationship indicated high drug-binding cooperativity (Fig. 1c). Further, Psora-4 exclusively inhibited Kv1.5 channels in the open state, with no indication of drug binding in the closed channel state (Fig. 1d).

Alanine-scanning mutagenesis of the Kv1.5 pore region

Alanine-scanning mutagenesis of the S6 segment and the pore helix in Kv1.5 channels was conducted to identify a potential Psora-4 binding site in the central pore cavity. This approach identified 11 mutations ('hits') in the S6 segment associated with markedly reduced inhibition by Psora-4 (Fig. 1e,f) and substantially increased IC_{50} values (up to 195-fold) (Supplementary Fig. 1). The hits comprised residues of the classical central cavity drug-binding site, including Thr480 in the pore helix and Val505, Ile508, Val512 and Val516 in the S6 segment (Fig. 1f,g). Mutation of two additional pore-lining alanine

residues (Ala501 and Ala509) to valine, previously reported to interfere with drug or Kvβ1.3 binding to the central cavity[14,15], also reduced Psora-4 inhibition (Fig. 1f,g). However, mutation of four residues (Ile502, Thr507, Leu510 and Pro513) that do not face the central cavity (Fig. 1f,g) also markedly reduced Psora-4 inhibition. Remarkably, these four residues point toward a hydrophobic cavity or side pocket formed by the backsides of S5 and S6 of a single subunit together with the S4 and S4–S5 linker of an adjacent subunit (Fig. 1g and Supplementary Fig. 2a).

A new drug-binding site in side pockets of Kv1.5

To explore whether Psora-4 indeed binds these side pockets, we alanine-scanned the lower S4 segment (Arg409 to Arg418), the complete S4–S5 linker (Gly419 to Q428A) and the lower S5 segment (Glu433 to Ser449). The scan revealed that four residues in the S4 segment (Ile410, Lys412, Leu413 and His416), four residues in the S4–S5 linker (Leu420, Leu423, Gly424 and Leu427) and six residues in the S5 segment (L437A, F439A, F440A, I443A, L447A and F448A) reduced block by Psora-4 (Fig. 1h,i) and substantially increased IC_{50} values (up to 276-fold) (Supplementary Fig. 1). Most of the identified residues are roughly located on the same side of the respective helices and face toward the side pockets postulated above and thus could potentially interact with Psora-4 occupying these side pockets (Supplementary Fig. 2b,c).

However, as mutations may cause nonspecific effects, several control experiments were performed. First, we tested whether the side-pocket mutants are also resistant to block by other drugs. Therefore, we tested the local anesthetic bupivacaine, a known Kv1.5 pore blocker. None of the mutations in the S4 segment or the S4–S5 linker reduced bupivacaine inhibition (Supplementary Fig. 3), indicating that the side-pocket cavities are binding sites for Psora-4 but not for all of the Kv1 blockers. Furthermore, although many mutations in S4 and the S4-S5 linker changed the extent of slow inactivation and/or shifted the voltage dependence of activation, there was no correlation between these parameters and Psora-4 inhibition (Supplementary Figs. 4 and 5). Collectively, these results argue strongly against nonspecific gating effects as the primary cause of the reduced Psora-4 sensitivity induced by mutation.

Modeling corroborates side pockets as binding sites

PAP-1, an analog of Psora-4, binds the central cavity of Kv1.3 such that two alkoxypsoralen molecules complex a K^+ ion in the T5 position under the selectivity filter, and the long flexible side chain protrudes into the intrasubunit interface between S5 and S6 (ref. 13). In contrast, our computational ligand dockings predict that Psora-4 should bind both the central cavity and the side pockets (Fig. 2a,b), interacting with the majority of residues identified by the mutagenesis scans (Supplementary Figs. 6 and 7). The contacts in the central cavity provided by the S6 segment are primarily hydrophobic in nature (Supplementary Fig. 6), with Val505, Ile508, Ala509, Val512 and Val516 all within close proximity (<4 Å) of the molecule (Fig. 2c and Supplementary Fig. 6). Psora-4 is positioned in close proximity to the selectivity filter, such that oxygen atoms of the furanocoumarin structure form hydrogen bonds with Thr480 of the pore signature sequence (Fig. 2c and Supplementary Fig. 6). The position of the molecule in the central cavity reduces the minimum aperture of the S6 gate

from 4 Å to 2.6 Å, which is sufficient to block K^+ ion conduction. For Psora-4 molecules docked into the side pockets, the interactions are primarily hydrophobic in nature (Fig. 2d and Supplementary Fig. 7). Residues within 4 Å of Psora-4 include Ile410 and Leu413 (S4); Leu420, Leu423, Gly424 and Leu427 (S4–S5 linker); Leu437, Phe440, Ile443, Leu447 and Phe448 (S5); and Thr507 and Leu510 (S6).

MDSs were performed to assess the dynamic interactions of the Kv1.5–Psora-4 complexes. In several independent 100-ns simulations, the protein stabilized to a typical Cα r.m.s. deviation between 3.5 Å and 4 Å, and the majority of contacts remained the same as described for the original docking. The MDSs validated almost all of the residues identified by the alanine scan and the molecular dockings (Supplementary Fig. 8a,b). Although Ala501 and Ile502 were too distant in the original docking, the increased flexibility during the subsequent MDSs allows Psora-4 to interact with these residues. Although the residues validated by MDSs mold the surface of the central cavity and the side pockets (Supplementary Fig. 8a,b), no contacts were observed with Lys412 (S4), His416 (S4) and Phe439 (S5). For Lys412 and His416, this apparent discrepancy might be caused by the state or conformation of the voltage sensor because a helical rotation, induced by the voltage sensor returning to its resting state, might enable the S4 residues Lys412 and His416 to interact with the Psora-4 molecule. This S4 flexibility is also in agreement with the less pronounced changes in IC_{50} for the S4 mutants (Supplementary Fig. 1). In summary, MDSs demonstrated that 22 out of the 25 residues identified by alanine-scanning mutagenesis are in sufficient spatial proximity to directly interact with the *in silico*–docked Psora-4.

Side pockets determine specificity and high cooperativity

The residues of the central drug-binding site are highly conserved within the different Kv families (Figs. 1a and 3a), whereas the protein sequence of the side pockets is only conserved within the Kv1 family (Supplementary Fig. 9). In oocytes, the IC_{50} of Psora-4 for Kv1.5 was 0.19 μM, whereas the IC_{50} for Kv2.1 was ~3.9 μM (Fig. 3b,c). The sequence of the drug-binding site of Kv1.5 differs from that of Kv2.1 at four residues in the side pockets and at two residues in the central cavity (Fig. 3a). We hypothesized that introducing a Kv1-like side pocket into Kv2.1 channels would enhance Psora-4 affinity. Indeed, four mutations introduced into Kv2.1 (Kv2.1 side pocket (SP)) to create a Kv1-like side pocket induced an approximately ten-fold increase in sensitivity to Psora-4 with an IC_{50} of 0.37 μM (Fig. 3a,c and Supplementary Fig. 10). This result suggests that drug binding to the side pockets is a crucial molecular determinant of high-affinity inhibition by Psora-4 and critically contributes to Kv1 specificity. As the Kv2.1 SP mutant lacks the high cooperativity of block (Fig. 3c), we additionally mutated the two residues differing in the central cavity drug-binding site (Kv2.1 SP+CC, where ‘CC’ stands for ‘central cavity’) (Fig. 3a and Supplementary Fig. 10). The Kv2.1 SP+CC mutant had a similar Psora-4 sensitivity (IC_{50} = 0.58 μM) as the Kv2.1 side-pocket mutant but had a much higher Hill coefficient (2.3) (Fig. 3c).

Co-expression of side-pocket mutants with wild-type channels caused a dominant-negative reduction of Psora-4 block (Supplementary Fig. 11), and, with the exception of I502A, all of the side-pocket and central cavity mutants that strongly reduced the potency of Psora-4 had

a Hill coefficient of about 1 (Fig. 3d illustrates an example of each segment). These findings suggest that the high cooperativity of inhibition depends on both binding sites harboring a Kv1-like sequence and that inhibition is highly dependent on 'cross-talk' between the central cavity and side-pocket binding sites. This interdependence is possible because when Psora-4 occupies the central cavity, it is in close proximity to Psora-4 in the side pockets, separated by just the S6 segment in a sandwich-like assembly (Fig. 3e), and both binding sites undergo conformational changes during channel activation (Supplementary Movie 1).

Psora-4 interacts with Ile502 of the lateral fenestrations

Wide lateral fenestrations were recently described in the crystal structure of a pre–open state of NavAb sodium channels, and it was suggested that these fenestrations might affect drug affinity[3]. Small lateral fenestrations between the S5 and S6 segment, also evident in the rKv1.2 crystal structure, might allow diffusion of Psora-4 or other drugs into the central cavity from the membrane phase. Alternatively, Psora-4 could also access the side pockets from the central cavity. Notably, Ile502 faces into this putative access pathway between the side pockets and the central cavity (Fig. 3f). The I502A mutation strongly reduced Psora-4 inhibition and had almost no effect on the Hill coefficient (Fig. 3d), but MDSs indicated only moderate counts of contact between the compound and this residue. Thus, Ile502 may not directly contribute to the binding sites or interfere with interdependence between the two binding sites. Instead, the I502A mutation might disturb the movement of Psora-4 between the central cavity and side pockets and thereby reduce drug affinity.

Psora-4 in the side pockets interacts with the pore helix

Some of our 100-ns MDSs predicted that Psora-4 bound in the side pockets can adopt a conformation in which the phenyl ring at the end of the alkyl side chain can reach up to the pore helix (Fig. 4a), and interactions with the key residues identified by mutagenesis were preserved. In addition, a large number of contacts were observed with Met478, which is located one amino acid before the pore signature sequence of Kv channels (MTTVGYG). Thus, we alanine-scanned the pore helix (Phe471 to Met478) and found that the W473A, V476A and M478A mutations strongly reduced Psora-4 affinity (Fig. 4b,c and Supplementary Fig. 12). Control experiments showed that the affinity of the nonspecific blocker bupivacaine was not changed for any of the pore helix mutants (Fig. 4d). In dockings where Psora-4 could interact with the pore helix, the MDSs also predicted an interaction with the non–pore-facing S6 segment residue Ala503. The A503V mutant had only a minor change in Psora-4 affinity (Fig. 1f). Thus, we introduced larger residues at this position (isoleucine and leucine) and found a strongly decreased Psora-4 affinity, with an almost 100-fold increased IC_{50} for the A503L mutant (Fig. 4e,f). Our data indicate that the Psora-4 alkyl side chain, together with the connected phenyl ring, intercalate between S5 and S6 to reach the pore helix (Fig. 4g). This binding mode might explain why the length of the alkyl side chain is crucial for the affinity of Psora-4 (ref. 12). It should be noted that the name Psora-4 indicates that the alkyl side chain connecting the phenyl ring has an optimal length of four CH_2 groups[12]. In the A503L mutant, the phenyl ring of Psora-4 might not be able to intercalate between S5 and S6 and reach the pore helix owing to spatial hindrance caused by this large moiety (Fig. 4h). Together, our findings suggest that Psora-4 interactions with the pore helix might be a critical determinant for the inhibitory mechanism.

Psora-4 does not modify channel gating or coupling

The Psora-4 binding site includes residues homologous to 'ILT' residues of S4 (ref. 16) and the 'internal cluster' residues of S5 in Shaker[17], for which mutants were described to cause an uncoupling from voltage sensing (Supplementary Fig. 13). However, as Psora-4 did not alter the kinetics of on or off gating currents or the charge-voltage (Q-V) relationship (Fig. 5a and Supplementary Table 4) or the conductance-voltage (G-V) relationship (Supplementary Fig. 14) of Kv1.5, we can conclude that the inhibitory mechanism does not involve electromechanical uncoupling or modification of channel activation. The observation that the S4 seems to remain flexible is also in agreement with our finding that Psora-4 can adopt different binding modes in the side pockets to reach the pore helix.

Stable inactivated drug–channel complex

To gain insights into the mechanism of Psora-4 inhibition, we studied Kv1.5 channels in inside-out macropatches (Fig. 5b–h) and observed a large increase in potency compared to drug application on whole oocytes. Almost complete inhibition is achieved with only 10 nM of Psora-4 by accumulating the inhibition from a large number of depolarizing steps (Fig. 5b, left). Furthermore, when Psora-4 is applied at higher concentrations (for example, 100 nM), we observed a time-dependent inhibition typical of open-state dependent block, and full inhibition was achieved during a single 2-s depolarizing pulse (Fig. 5b, right). Thus, in the macropatch recordings, but not in intact oocytes, a clear open state–dependent block was observed. As lower apparent potencies are seen especially for lipophilic compounds in oocytes compared to inside-out macropatches, this apparent discrepancy is most likely reflected by the drug available at the inner opening of the channel mouth. Psora-4 might be able to rapidly enter its binding sites through the open channel in the macropatch configuration but is sequestered into cytoplasmic hydrophobic compartments in oocytes, resulting in a low free Psora-4 concentration and, thus, slow drug-binding rates that cannot be separated from slow inactivation in these channels (as with the inside-out patch with 10 nM Psora-4 in Fig. 5b). As is typical for an open channel blocker, the kinetics of blocking were dependent on the drug concentration (Fig. 5b, right). However, whereas most open channel blockers unbind from the channel upon repolarization within milliseconds, Psora-4 unbinding was extremely slow. In the presence of drug inhibition, little recovery at −80 mV was observed, and, even upon drug removal, the current recovered only partially after 30 min (Fig. 5c).

The kinetics for the onset of Kv1.5 block were not changed for the side-pocket mutants L423A and T507A, but they were greatly slowed by the mutation I508A, located in the central cavity (Fig. 5d). Thus, the rapid onset of block seen at higher concentrations most likely results from Psora-4 binding to the central cavity. In contrast, whereas recovery from inhibition of wild-type channels was extremely slow, all three of the mutant channels had a remarkably fast recovery from inhibition that was complete within the 12-s interpulse interval (Fig. 5d; T507A not illustrated). Thus, the mutations studied here seem to primarily interfere with the formation of a stable drug–channel complex formed in the open state that requires high-affinity binding to both the central cavity and the side-pocket binding sites.

Next, we tested whether the pore blocker tetraethyl-ammonium (TEA)[18] interfered with Psora-4 binding in the central cavity. TEA (3 mM) slowed the kinetics of block as though TEA-blocked channels were less sensitive to Psora-4 inhibition (Fig. 5e). This effect was also evident when high TEA concentrations (100 mM) were present during a long depolarizing pulse, as this prevented the otherwise complete inhibition by 100 nM Psora-4 (compare second pulse in Fig. 5f and third pulse in Fig. 5g). The insensitivity of TEA-blocked channels to Psora-4 could be a result of direct competition as TEA and Psora-4 probably cannot simultaneously occupy the central cavity. Alternatively, TEA is known to stabilize the selectivity filter and can thereby slow C-type inactivation in Kv channels[19]. Thus, TEA might prevent the formation of a stable, inactivated channel complex with Psora-4. As the larger triethyl-butyl-ammonium (TEA-C_4) or tetrapentyl-ammonium (TPA) also compete with pore blockers and have a similar fast wash-out but do not interfere with C-type inactivation[19], we tested TPA under the same conditions (Fig. 5h). With TPA, there is no apparent competition, and the pulse after TPA removal (Fig. 5h, third pulse) is identical to that for wild-type channels that were previously blocked by Psora-4 (Fig. 5f, third pulse). This apparent lack of competition in the central cavity suggests that Psora-4 in the side pockets can induce an inactivated state while TPA is present in the central cavity (Fig. 5h, cartoon second pulse). In addition, this nonconducting inactivated state persists when the pore-plugging molecule (here TPA) has been removed from the central cavity (Fig. 5h, cartoon third pulse). Remarkably, the interaction of Psora-4 with the pore helix (Fig. 4) might induce an inactivation-like process at the selectivity filter that is critical for the formation of a stable nonconducting state of the Psora-4–channel complex.

DISCUSSION

We propose that a single Psora-4 molecule binds the conserved central cavity, whereas up to four additional drug molecules can bind the side pockets of Kv1 channels. Psora-4 in the central cavity acts as a typical pore blocker and physically prevents K^+ permeation. However, the high affinity and high cooperativity of block and the selectivity for Kv1 channels seems to be dependent on Psora-4 molecules bound to one or more side pockets. Co-expression of side-pocket mutants with wild-type channels exerts a dominant-negative reduction of Psora-4 block, suggesting that several side pockets need to bind Psora-4 in a proper way to enable the allosteric inhibition of Kv1.5. In addition, we observed a mechanistically important interaction of the drug with the pore helix, suggesting that the Psora-4 molecules in the side pockets might induce an inactivation-like mechanism by ‘pushing’ on the backside of the selectivity filter. In other words, our data suggest that Psora-4 (or TPA) needs to be present in the central cavity for Psora-4 molecules bound to the side pocket (or pockets) to induce an extremely stable inactivated drug-channel complex. Furthermore, it is known that non–pore-facing residues in the S5 and S6 are critical for drug inhibition of Ca^{2+} and Na^+ channels[20–22], suggesting that side-pocket drug interactions might have general relevance for the pharmacology of voltage-gated ion channels. The sequence conservation in the side pockets of voltage-gated Ca^{2+} and Na^+ channels is very low in comparison to that in Kv channels. Thus, side pockets might also provide the opportunity to develop specific drugs targeting different Na^+ and Ca^{2+} channel isoforms. Unlike in Kv channels, which most commonly form tetramers with identical subunits, the

four side pockets of the covalently linked Na^+ and Ca^{2+} channel tetramers vary even within a specific isoform. This increased sequence variability in the side pockets of Na^+ and Ca^{2+} channels might provide a very promising opportunity for the design of specific drugs but conversely might also hinder the simultaneous occupation of all four of the side pockets by a single type of molecule.

The side-pocket sites described here for Kv1 are also present in other voltage-gated channels. As the residues that form the side pockets are less conserved than those lining the pore, this structure represents a promising new target for development of new, highly selective channel inhibitors. Furthermore, drugs that specifically bind the side pockets might increase the efficacy of known central pore blockers.

METHODS

Methods and any associated references are available in the online version of the paper.

ONLINE METHODS

Molecular biology

The used Kv1.5 (*KCNA5*) cDNA construct was previously described[6]. The PCR-based site directed mutagenesis QuikChange (Stratagene) was used to insert mutations into the human Kv1.5 cDNA. PCR products were fully sequenced (ABI 3100, Applied Biosystems). For the injection into *Xenopus laevis* oocytes, Kv1.5 cDNA was linearized with *Nhe1*, and complementary RNA (cRNA) was assembled with the mMESSAGE mMACHINE T7-Kit (AM1344, Ambion). cRNA quality was determined by gel electrophoresis and UV spectroscopy.

TEVC measurements

Kv1.5 wild-type or mutant cRNA was injected into isolated stage IV and V *X. laevis* oocytes. After injection, they were cultured in bath solution comprising 88 mM NaCl, 1 mM KCl, 0.4 mM $CaCl_2$, 0.33 mM $Ca(NO_3)_2$, 1 mM $MgSO_4$, 2.4 mM $NaHCO_3$, 10 mM HEPES, pH 7.4, supplemented with 50 μg/ml gentamycine and 1 mM pyruvate at 18 °C for 1–13 d before the experiments. During the two-electrode voltage clamp (TEVC) experiments, we used a modified ND96 solution that contained: 96 mM NaCl, 4 mM KCl, 1 mM $MgCl_2$, 1 mM $CaCl_2$, 5 mM HEPES, pH 7.5. The test protocol comprises test pulses to +40 mV for 2 s at intervals of 10 s from a holding potential of −80 mV. Psora-4 was synthesized at the chemical department of Sanofi-Aventis GmbH Germany and prepared as a 10-mM stock solution in DMSO and stored at room temperature. To obtain the concentration of the compound blocking 50% of the current (IC_{50}), a Hill plot was used, based on 2–5 concentrations on 3–22 oocytes/point. Data are represented throughout the figures as mean ± s.e.m. (***$P < 0.001$). Biophysical parameters of the mutants studied, including $V_{1/2}$ of activation, time constants of activation (τ_{act}), time constants of inactivation (τinact) and extent of inactivation at +40 mV (% inact.) are provided in Supplementary Tables 2 and 3. $V_{1/2}$ for activation was determined with tail current analysis at −40 mV as previously decribed[15]. For mutant channels with small tail current amplitudes, we determined the $V_{1/2}$ by correcting the peak current amplitudes by the driving force before

fitting to a Boltzmann equation. These mutants are indicated in Supplementary Table 2 by a hash symbol. Note that the time constants from a monoexponential fit of inactivation over a time period of 2 s provide only an approximation of the inactivation kinetics. Asterisks in Supplementary Table 2 indicate data obtained from a previous study[15].

Homology modeling

Modeller 9v5 (ref. 23) was used to create homology models of Kv1.5 (Swiss-Prot[24] ID: P22460) based on the crystal structures of the open state Kv1.2:Kv2.1 chimera (KvChim) (Protein Data Bank (PDB) code 2R9R) and the closed state MlotiK channel (PDB code 3BEH). The KvChim-based model was modeled from S1 to S6, with residues 285–299 and 381–388 omitted from the S1-S2 and S3-S4 extracellular linkers, respectively. As the MlotiK channel is not a voltage-gated channel, the model based on this structure consists of only S4 to S6. Four-fold symmetry was applied to the models. The final Kv1.5 models were compared to their crystal structure template to verify that the modeling step had not altered backbone and side chain conformations.

Ligand docking

The ligand molecule was drawn using Marvin (v5.0.2.1, 2008, ChemAxon (http://www.chemaxon.com/)). Ligand dockings were performed using both GOLD and AutoDock (v4)[25]. Initially a large cubic grid was specified, incorporating both binding sites. A second search was then performed, focused on either the central cavity or the region above the S4-S5 linker. For each docking, ten solutions were generated, from which the best-ranked solution was selected. Binding orientations were visualized using PyMOL v1.2 (http://www.pymol.org/).

Molecular dynamics simulations

Molecular dynamics simulations (MDSs) were performed on the Kv1.5 homology models based on KvChim and embedded in a POPC lipid bilayer. K^+ ions were either placed at S_2 and S_4 of the selectivity filter of the Kv1.5 homology models, with water molecules placed at the sites not occupied by ions[26,27]. The initial coordinates of the ligand in the simulations were based on the best-ranked conformations from the Autodock results. Four simulations were performed with Psora-4 (i) present in all five cavities, (ii) present in only the four side cavities, (iii) present only in the central cavity or (iv) not present. The models were positioned in a POPC membrane bilayer, with any overlapping lipids removed. The central cavity of the channel was solvated, in the presence of the ligand molecule, using the programs Voidoo and Flood[28]. The remainder of the system above and below the bilayer was solvated using the Gromacs software suite. Cl^- ions were added at random within the solvent to neutralize the system. The periodic box surrounding the ~73,500-atom system was ~$9 \times 9 \times 11$ nm^3. The parameters for the ligand molecule were generated using the PRODRG server[29]. The partial charges were generated using Maestro (v8.5).

MDSs were performed with Gromacs (v4.0.7)[30] (http://www.gromacs.org/) using the GROMOS96 43a1 force field[31]. Simulations were performed using semi-isotropic pressure coupling with the Parrinello-Rahman barostat[32]. The temperature of the system was coupled to an external bath held at 300 K, using the V-rescale thermostat. The water model used was

SPC[33]. LINCS was used to constrain bond lengths[34]. Long-range electrostatics, up to 10 Å, were modeled using the Particle Mesh Ewald (PME) method. A cutoff of 10 Å was also used for van der Waals interactions. Gromacs was used to add polar hydrogen atoms to the protein structure. In four 100-ns simulations (one without drug, and three with drug), the protein stabilized to a typical Cα r.m.s. deviation of between 3.5 Å and 4 Å. In the three simulations that contained the Psora-4 molecule, the complexes remained intact for the duration of the simulation. The percentage of contacts for each protein side chain within 4 Å of the drug molecule was calculated at 10-ps intervals for all three ligand-containing simulations.

Each system was initialized with a steepest-descents energy minimization step, followed by 1 ns of restrained MD in which the nonhydrogen protein atoms and K^+ ions were restrained with a force constant of 1,000. All four systems were subjected to 100 ns of unrestrained MD, during which coordinates were saved every 10 ps for analysis. Additional simulations were run for 50 ns, with only Psora-4, a POPC lipid bilayer and solvent. Analysis of the simulations was performed using Gromacs, VMD (v1.8.6) and locally written code[35].

COVG measurements

Gating currents of W472F Kv1.5 (nonconducting) channels were measured with the cut-open oocyte Vaseline gap (COVG) recording technique[36]. The COVG chamber consists of three compartments (upper, guard and bottom) that are isolated from one another by Vaseline seals. Microelectrodes were pulled from borosilicate glass capillary tubes to obtain resistances of 0.1–0.5 MΩ when filled with 3 M KCl and were used to record the transmembrane potential of the oocyte domus protruding into the upper compartment. Electrical access to the cytoplasm was obtained by permeabilizing the portion of the oocyte isolated in the bottom compartment with 0.3% saponin for 2 min.

A CA-1B amplifier (Dagan, Minneapolis), Digidata 1322A data acquisition system (Axon Instruments, Union City, CA) and a personal computer were configured to voltage clamp an oocyte with command voltage pulses generated with PCLAMP8 software (Axon Instruments). Signals were low pass–filtered at 10 kHz and digitized at 40 kHz. Linear leak and capacitance currents were compensated by analog circuitry and subtracted on-line by using a p/−8 protocol[37]. The holding potential was −90 mV, and the test pulse duration was 20 ms. Leak and capacitance currents were on-line subtracted using −P/8 protocol. Recordings were performed at room temperature (22–24 °C) under no-flow conditions.

Gating currents were recorded using an extracellular solution in the top and guard compartments that contained: 96 mM NaCl, 4 mM KCl, 1 mM $CaCl_2$, 1 mM $MgCl_2$ and 5 mM HEPES; the pH was adjusted to 7.6 with NaOH. The extracellular solution in the top and guard compartments for measurement of gating currents contained: 120 mM NMDG-MES, 2 mM Ca-MES, 10 mM HEPES, pH 7.4. The intracellular solution in the bottom compartment contained: 120 mM NMDG-MES, 2 mM EDTA and 10 mM HEPES, pH 7.4.

Inside-out macropatch clamp experiments from *Xenopus* oocytes

Giant patch recordings in the inside-out configuration under voltage-clamp conditions were made at room temperature 3–5 d after cRNA injection. Pipettes were made from thick-

walled borosilicate glass, had resistances of 0.3–0.9 M (tip diameter of 5–15 μm) and were filled with: 120 mM KCl, 10 mM HEPES and 1.8 mM $CaCl_2$; the pH was adjusted to 7.2 with KOH. Currents were recorded with an EPC9 or EPC10 amplifier (HEKA electronics, Lamprecht, Germany) and sampled at 10 kHz with analog filter set to 3 kHz (−3 dB). Currents from Kv1.5 channels were elicited by double pulses from −80 mV (holding potential) to +40 mV with various interpulse intervals as indicated in Figure 5. Internal solution (K_{int}) was applied to the cytoplasmic side of excised patches via a multibarrel pipette and had the following composition: 120 mM KCl, 10 mM HEPES, 2 mM K_2EGTA; the pH was adjusted to 7.2. Psora-4 was stored as a stock solution of 10 mM in DMSO at room temperature and diluted in K_{int} to the final concentration. Kinetics of blocking were ana-lyzed with a monoexponential fit of the first pulse in the presence of Psora-4. Note that the kinetics of Kv1.5 inhibition by 100 nM Psora-4 was faster in the experiment shown in Figure 5d (τ = 103 ± 30 ms) compared to that shown in, for example, Figure 5e (τ = 211 ± 41 ms). We observed some variability in Psora-4 inhibition, depending on the patch, which most likely reflects differences in the amount of cytoskeleton and yolk excised with the patch (presumably absorbing some Psora-4). The variability seemed to depend on the batch of oocytes. Thus, comparison of drug inhibition was most consistent when wild-type and mutant channels were measured on the same day and from the same oocyte preparation.

Data analysis

For data analyses, PClamp 8 (Molecular Devices) and Origin 7 (Microcal Software) software were used. All fitting procedures were based on the simplex algorithm. Integration of ON gating current (Ig_{ON}) elicited by membrane depolarization was used to calculate the ON intramembrane charge displacement (Q_{ON}). Integration of the OFF gating current (Ig_{OFF}) induced by subsequent repolarization was used to calculate the OFF intramembrane charge displacement (Q_{OFF}). The charge-voltage (Q-V) relationship for each oocyte was normalized to the maximum value of Q under control conditions determined from fitting the data to a Boltzmann function: where $V_{1/2}$ is the half-point of the relationship and *z* is the effective valence.

Statistical analysis

Results are reported as mean ± s.e.m. (*n* = number of oocytes). Significance was probed using an unpaired two-tailed Students *t*-test with a *P* value of <0.001.

Supplementary Material

Refer to Web version on PubMed Central for supplementary material.

Acknowledgments

This work was supported by Deutsche Forschungsgemeinschaft grant DE1482-3/2 to N.D. and by the P.E. Kempkes Stiftung 01/2011 to S.R. and S.M. M.S.P.S. is supported by the Wellcome Trust. M.C.S. was supported by US National Institutes of Health (NIH)–NIH Heart, Lung, and Blood Institute grant HL055236. S.M. was supported by the Studienstiftung des Deutschen Volkes e.V.

References

1. Wulff H, Castle NA, Pardo LA. Voltage-gated potassium channels as therapeutic targets. Nat Rev Drug Discov. 2009; 8:982–1001. [PubMed: 19949402]
2. Hockerman GH, Dilmac N, Scheuer T, Catterall WA. Molecular determinants of diltiazem block in domains IIIS6 and IVS6 of L-type Ca^{2+} channels. Mol Pharmacol. 2000; 58:1264–1270. [PubMed: 11093762]
3. Payandeh J, Scheuer T, Zheng N, Catterall WA. The crystal structure of a voltage-gated sodium channel. Nature. 2011; 475:353–358. [PubMed: 21743477]
4. Ragsdale DS, McPhee JC, Scheuer T, Catterall WA. Common molecular determinants of local anesthetic, antiarrhythmic, and anticonvulsant block of voltage-gated Na^+ channels. Proc Natl Acad Sci USA. 1996; 93:9270–9275. [PubMed: 8799190]
5. Ragsdale DS, McPhee JC, Scheuer T, Catterall WA. Molecular determinants of state-dependent block of Na^+ channels by local anesthetics. Science. 1994; 265:1724–1728. [PubMed: 8085162]
6. Decher N, et al. Molecular basis for Kv1.5 channel block: conservation of drug binding sites among voltage-gated K^+ channels. J Biol Chem. 2004; 279:394–400. [PubMed: 14578345]
7. Mitcheson JS, Chen J, Lin M, Culberson C, Sanguinetti MC. A structural basis for drug-induced long QT syndrome. Proc Natl Acad Sci USA. 2000; 97:12329–12333. [PubMed: 11005845]
8. Seebohm G, et al. Molecular determinants of KCNQ1 channel block by a benzodiazepine. Mol Pharmacol. 2003; 64:70–77. [PubMed: 12815162]
9. Hanner M, et al. Binding of correolide to the Kv1.3 potassium channel: characterization of the binding domain by site-directed mutagenesis. Biochemistry. 2001; 40:11687–11697. [PubMed: 11570869]
10. MacKinnon R, Heginbotham L, Abramson T. Mapping the receptor site for charybdotoxin, a pore-blocking potassium channel inhibitor. Neuron. 1990; 5:767–771. [PubMed: 1702643]
11. Swartz KJ, MacKinnon R. Mapping the receptor site for hanatoxin, a gating modifier of voltage-dependent K^+ channels. Neuron. 1997; 18:675–682. [PubMed: 9136775]
12. Vennekamp J, et al. Kv1.3-blocking 5-phenylalkoxypsoralens: a new class of immunomodulators. Mol Pharmacol. 2004; 65:1364–1374. [PubMed: 15155830]
13. Zimin PI, et al. Potassium channel block by a tripartite complex of two cationophilic ligands and a potassium ion. Mol Pharmacol. 2010; 78:588–599. [PubMed: 20601455]
14. Decher N, et al. Structural determinants of Kvβ1.3-induced channel inactivation: a hairpin modulated by PIP_2. EMBO J. 2008; 27:3164–3174. [PubMed: 18987637]
15. Decher N, Kumar P, Gonzalez T, Renigunta V, Sanguinetti MC. Structural basis for competition between drug binding and Kvβ1.3 accessory subunit-induced N-type inactivation of Kv1.5 channels. Mol Pharmacol. 2005; 68:995–1005. [PubMed: 16024663]
16. Ledwell JL, Aldrich RW. Mutations in the S4 region isolate the final voltage-dependent cooperative step in potassium channel activation. J Gen Physiol. 1999; 113:389–414. [PubMed: 10051516]
17. Soler-Llavina GJ, Chang TH, Swartz KJ. Functional interactions at the interface between voltage-sensing and pore domains in the *Shaker* Kv channel. Neuron. 2006; 52:623–634. [PubMed: 17114047]
18. Armstrong CM, Hille B. The inner quaternary ammonium ion receptor in potassium channels of the node of Ranvier. J Gen Physiol. 1972; 59:388–400. [PubMed: 4112955]
19. Baukrowitz T, Yellen G. Two functionally distinct subsites for the binding of internal blockers to the pore of voltage-activated K^+ channels. Proc Natl Acad Sci USA. 1996; 93:13357–13361. [PubMed: 8917595]
20. Huber I, et al. Conserved Ca^{2+}-antagonist-binding properties and putative folding structure of a recombinant high-affinity dihydropyridine-binding domain. Biochem J. 2000; 347:829–836. [PubMed: 10769189]
21. Nau C, Wang GK. Interactions of local anesthetics with voltage-gated Na^+ channels. J Membr Biol. 2004; 201:1–8. [PubMed: 15635807]

22. Striessnig J, et al. Structural basis of drug binding to L Ca^{2+} channels. Trends Pharmacol Sci. 1998; 19:108–115. [PubMed: 9584627]
23. Šali A, Blundell TL. Comparative protein modelling by satisfaction of spatial restraints. J Mol Biol. 1993; 234:779–815. [PubMed: 8254673]
24. Boeckmann B, et al. The SWISS-PROT protein knowledgebase and its supplement TrEMBL in 2003. Nucleic Acids Res. 2003; 31:365–370. [PubMed: 12520024]
25. Goodsell DS, Morris GM, Olson AJ. Automated docking of flexible ligands: applications of AutoDock. J Mol Recognit. 1996; 9:1–5. [PubMed: 8723313]
26. Åqvist J, Luzhkov V. Ion permeation mechanism of the potassium channel. Nature. 2000; 404:881–884. [PubMed: 10786795]
27. Zhou Y, Morais-Cabral JH, Kaufman A, MacKinnon R. Chemistry of ion coordination and hydration revealed by a K^+ channel–Fab complex at 2.0 Å resolution. Nature. 2001; 414:43–48. [PubMed: 11689936]
28. Kleywegt GJ, Jones TA. Detection, delineation, measurement and display of cavities in macromolecular structures. Acta Crystallogr D Biol Crystallogr. 1994; 50:178–185. [PubMed: 15299456]
29. van Aalten DM, et al. PRODRG, a program for generating molecular topologies and unique molecular descriptors from coordinates of small molecules. J Comput Aided Mol Des. 1996; 10:255–262. [PubMed: 8808741]
30. Van Der Spoel D, et al. GROMACS: fast, flexible, and free. J Comput Chem. 2005; 26:1701–1718. [PubMed: 16211538]
31. Scott WRP, et al. The GROMOS biomolecular simulation program package. J Phys Chem A. 1999; 103:3596–3607.
32. Parrinello M, Rahman A. Polymorphic transitions in single-crystals—a new molecular-dynamics method. J Appl Phys. 1981; 52:7182–7190.
33. Hermans J, Berendsen HJC, Vangunsteren WF, Postma JPM. A consistent empirical potential for water-protein interactions. Biopolymers. 1984; 23:1513–1518.
34. Hess B, Bekker H, Berendsen HJC, Fraaije JGEM. LINCS: a linear constraint solver for molecular simulations. J Comput Chem. 1997; 18:1463–1472.
35. Humphrey W, Dalke A, Schulten K. VMD: visual molecular dynamics. J Mol Graph. 1996; 14:33–38. [PubMed: 8744570]
36. Stefani E, Bezanilla F. Cut-open oocyte voltage-clamp technique. Methods Enzymol. 1998; 293:300–318. [PubMed: 9711615]
37. Armstrong CM, Bezanilla F. Inactivation of the sodium channel. II. Gating current experiments. J Gen Physiol. 1977; 70:567–590. [PubMed: 591912]

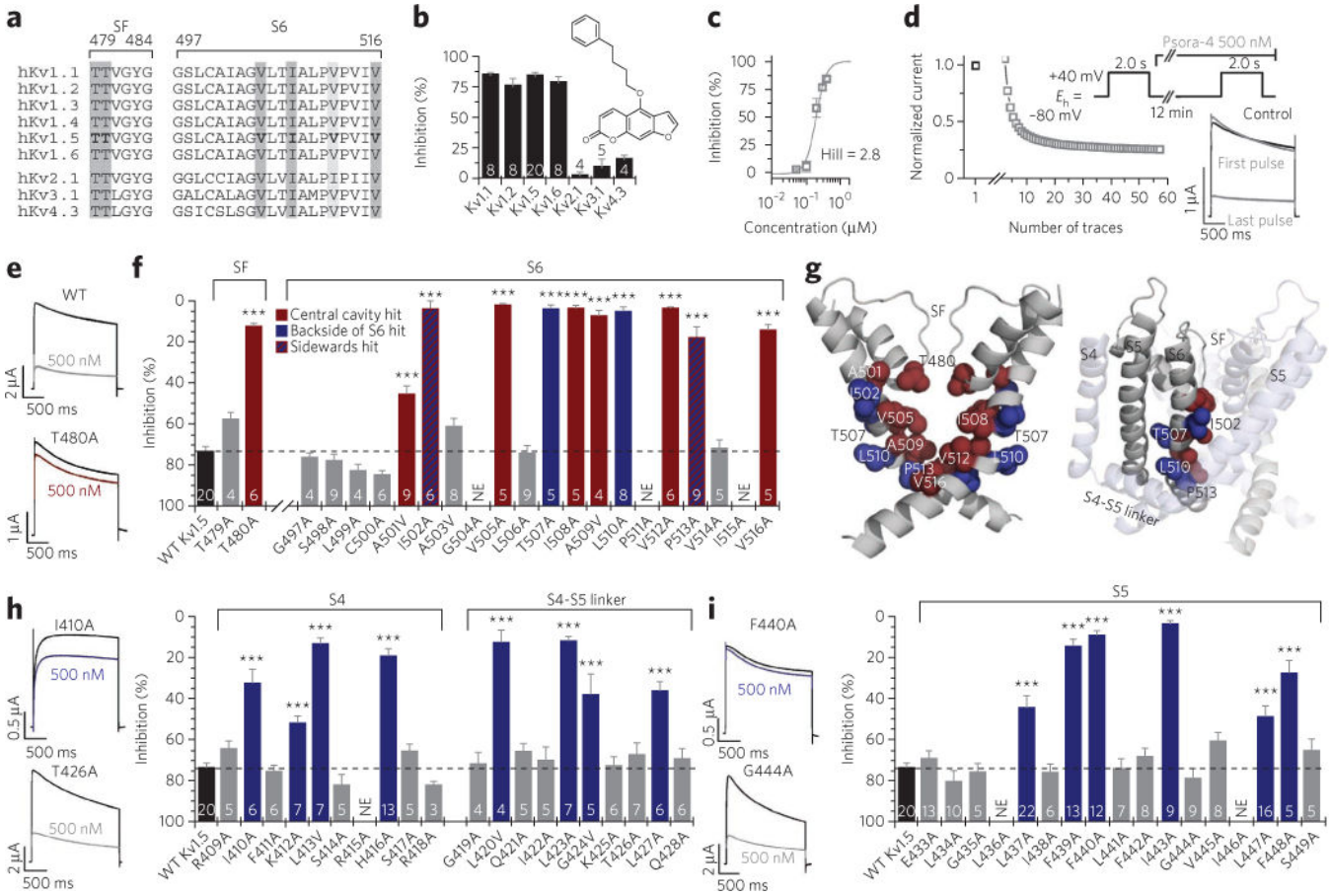

Figure 1. Identification of pore-facing and non–pore-facing amino acids of the Psora-4 binding site

(**a**) Alignment of the pore helix and pore forming S6 segment of Kv channels. The classical drug-binding site is highlighted in gray. SF, selectivity filter. (**b**) Block of different Kv channels by 500 nM Psora-4, analyzed at +40 mV. Inset shows the structure of Psora-4. (**c**) Dose-response relationship for Kv1.5 channels. *n* = 7–20 per concentration. (**d**) Kv1.5 currents under control conditions and repetitive pulses directly after a 12-min pulse-free period in the presence of 500 nM Psora-4 (*n* = 7). The upper panel illustrates the voltage protocol, and the inset shows representative measurements. (**e**) Wild-type (WT) and mutant channel currents before and after incubation with 500 nM Psora-4. (**f**) Alanine scan of the S6 using 500 nM Psora-4, analyzed at +40 mV. SF, selectivity filter. (**g**) Localization of pore-facing and non–pore-facing residues in an open-state Kv1.5 homology model. (**h**,**i**) Alanine scan of the S4, S4-S5 linker (**h**) and the S5 segment (**i**). In **e**–**i**, red and blue coloring refers to pore-facing and non–pore-facing residues, respectively. Data are represented throughout the figure as mean ± s.e.m. The number of experiments (*n*) are indicated as small insets within the bars. $^{***}P < 0.001$. NE, not expressing.

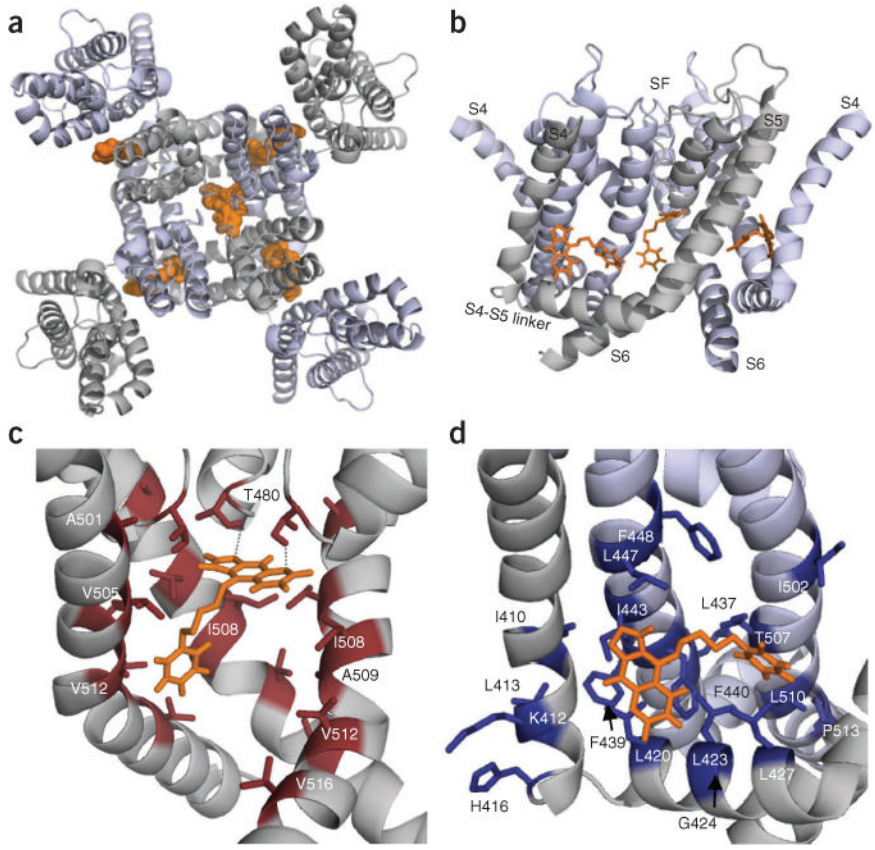

Figure 2. Psora-4 binding site in the central cavity and side pockets

(**a**,**b**) Kv1.5 open-state homology model with Psora-4 molecules shown in orange, viewed from the extracellular face (**a**) and from the side (**b**). (**c**,**d**) Docking of Psora-4 in the central cavity (**c**) and the side pockets (**d**). The residues identified by mutagenesis are shown as colored sticks (red, classical pore drug-binding site; blue, side-pocket binding site). The binding orientation for Psora-4, as predicted by GOLD, is shown in orange.

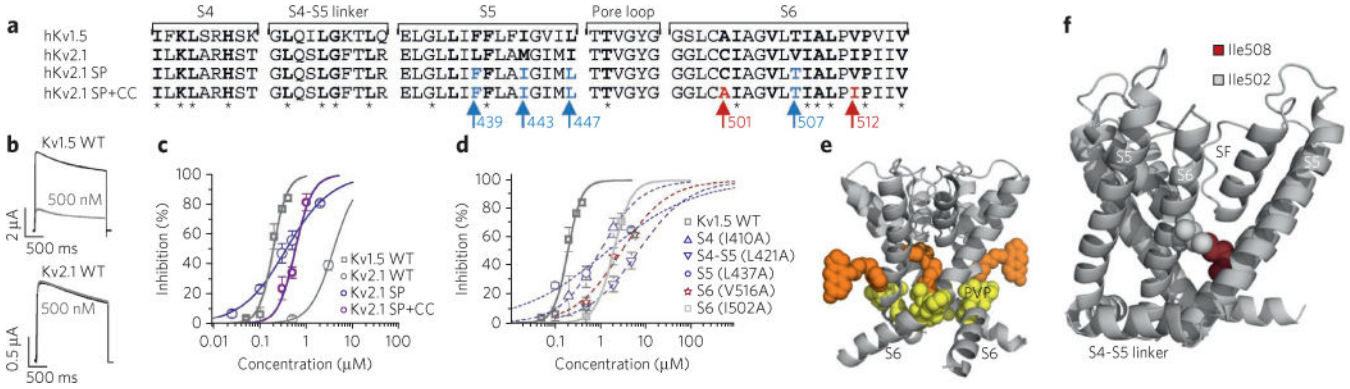

Figure 3. Introducing Psora-4 affinity into Kv2.1 channels by creating a Kv1-like side pocket

(**a**) Alignment of Kv1.5, Kv2.1, the four-fold mutant Kv2.1 SP and the six-fold mutant Kv2.1 SP+CC. The Psora-4 binding site is highlighted in bold. Asterisks indicate conserved residues of the binding site. The Kv2.1 mutations at the nonconserved sites are marked by arrows (red, central cavity; blue, side pocket). (**b**) Psora-4 effect on Kv1.5 and Kv2.1 channels expressed in oocytes. WT, wild type. (**c**) Dose-response curves of Kv1.5, Kv2.1, Kv2.1 SP and Kv2.1 SP+CC for Psora-4; n = 4–20 per concentration. (**d**) Examples of the dose-response relationships from binding-site mutant channels of each drug-binding domain; n = 3–22 per concentration. (**e**) Open pore homology model of Kv1.5, including the S6 and the pore loops of four subunits. Psora-4 molecules are shown in orange. One Psora-4 molecule is bound to the central cavity, and additional Psora-4 molecules are illustrated in two opposing side pockets. The proline-valine-proline (PVP) sequences are highlighted as yellow spheres. (**f**) Open pore homology model of Kv1.5 with Ile508 (red) facing the pore and Ile502 (light gray) facing the lateral fenestrations. SF, selectivity filter. Data are represented throughout the figure as mean ± s.e.m.

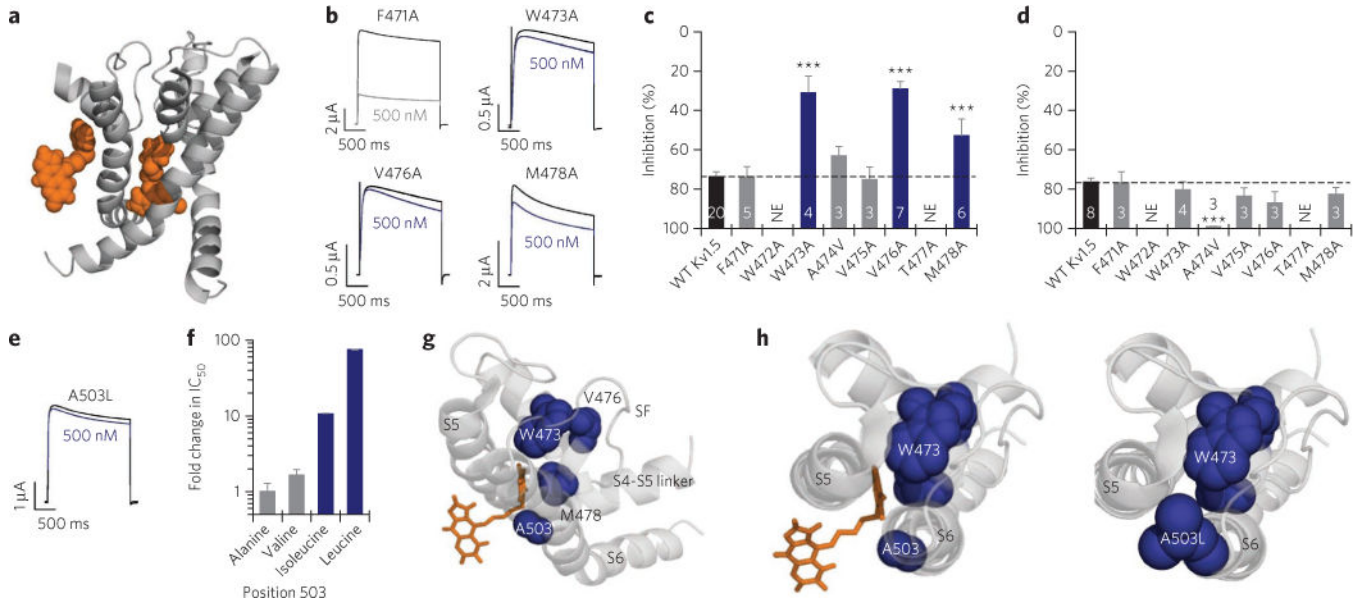

Figure 4. Psora-4 in the side pocket interacts with the pore helix

(**a**) MDS result where one Psora-4 molecule bound in the side pockets is reaching the pore helix. Psora-4 is shown in orange. (**b**) Mutant channel currents before and after incubation with 500 nM Psora-4. (**c**) Inhibition of pore helix mutants by 500 nM Psora-4, analyzed at +40 mV. WT, wild type. (**d**) Inhibition of pore helix mutant channels by 250 µM bupivacaine. In **c** and **d**, the number of experiments (*n*) are indicated within the bars. (**e**) Inhibition of A503L mutant by 500 nM Psora-4. (**f**) Fold changes in IC_{50} introducing different residues at position 503; *n* = 3–13 per concentration. (**g**) Residues of the pore helix and A503 (S6) that interact with Psora-4 are highlighted as blue spheres. (**h**) Large residues at position 503 (A503L) might interfere with Psora-4 access to the pore helix. Data are represented throughout the figure as mean ± s.e.m. $^{***}P < 0.001$. NE, not expressing.

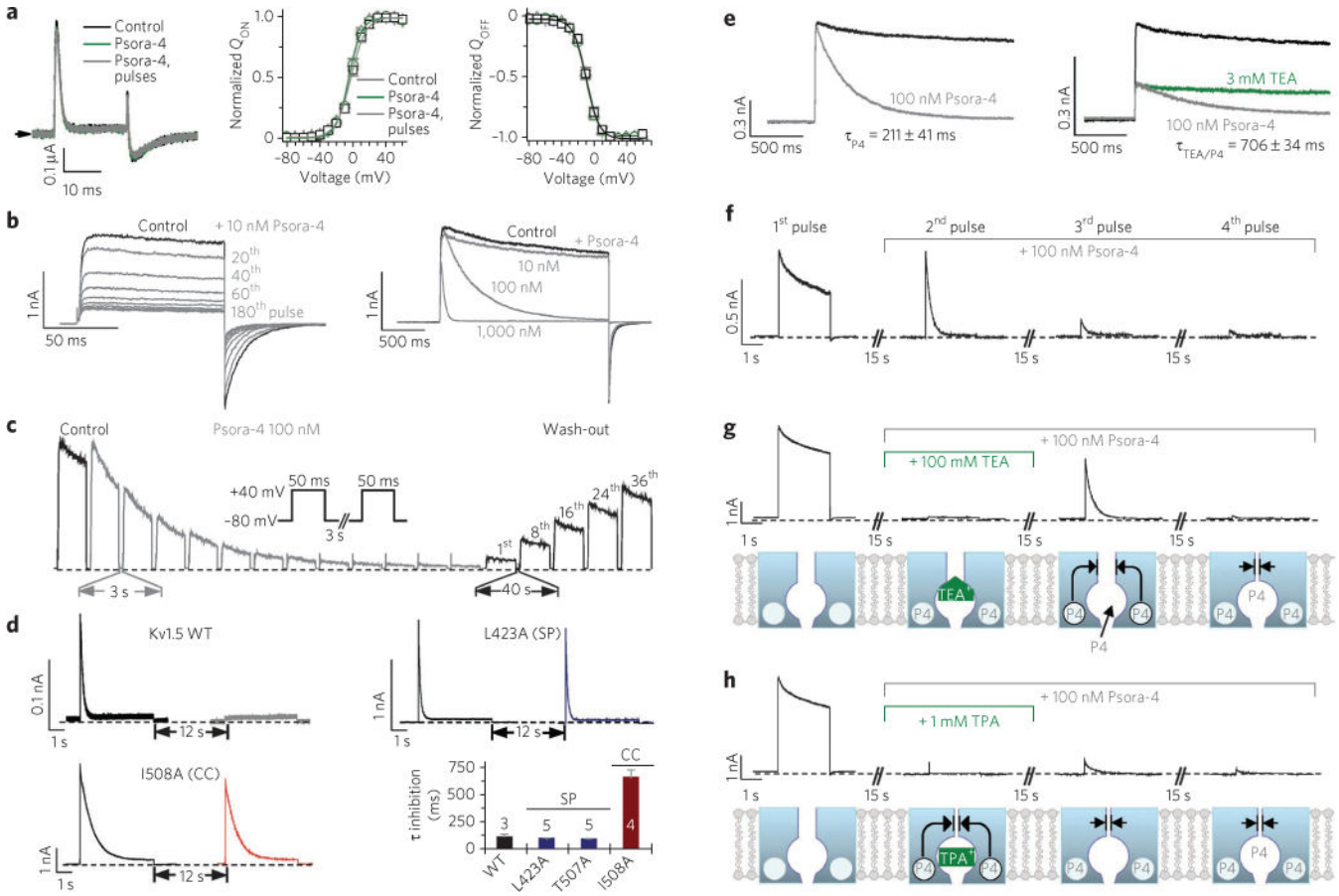

Figure 5. Psora-4 blocking mechanism

(**a**) Superimposed Kv1.5 gating currents recorded at +60 mV before (control) and after addition of 500 nM Psora-4 for 15 min without pulsing (Psora-4) and after 20 pulses to +60 mV (Psora-4, pulses). Middle and right panels illustrate the Q_{ON} and Q_{OFF} voltage relationships (n = 5). (**b**–**h**) Inside-out macropatch recordings from *Xenopus* oocytes. (**b**) Inhibition of Kv1.5 by low Psora-4 doses (left) and block by different Psora-4 concentrations (right). (**c**) Time course of wash-in and wash-out of 100 nM Psora-4. (**d**) Time course of inhibition and reversibility of block for drug-binding site mutations in the central cavity (CC, red) and side pocket (SP, blue). After the control pulse (not shown), patches were incubated with 100 nM Psora-4 for 3 min. The first and second pulse in the presence of Psora-4 are illustrated. Kinetics of block were analyzed with a monoexponential fit (see Online Methods for batch-dependent analyses). (**e**) The kinetics of block by Psora-4 in the absence (left; n = 4) and presence of TEA (right; n = 3). τ_{P4} is the time constant of inhibition by Psora-4. (**f**) Inside-out patch clamp recordings of Psora-4 alone or after pre-application of either TEA (**g**) or TPA (**h**). In **g** and **h**, the models depict the occupancy of the different binding sites by Psora-4 (P4), the competition of the binding in the central cavity and the proposed effects on the selectivity filter. The triangular shape of TEA indicates the stabilization of the selectivity filter. The arrows mark the stable pore collapse. Data are represented as mean ± s.e.m.